Optimization of Second Harmonic Generation and Nonlinear Phase-Shifts in the Čerenkov Regime

Gijs J. M. Krijnen, *Member, IEEE*, William Torruellas, *Member, IEEE*, George I. Stegeman, *Member, IEEE*, Hugo J. W. M. Hoekstra, *Member, IEEE*, and Paul V. Lambeck

***Abstract*—We present Beam Propagation Method (BPM) studies of Second Harmonic Generation (SHG) and nonlinear phase-shifts by cascading. The studies concentrate on SHG by means of radiation modes; the Čerenkov regime. The presented modeling does take into account both depletion and nonlinear phase shifts of the fundamental fields. BPM results show that leaky waves play an important role offering possibilities for enhancing the efficiency of SHG by orders of magnitude over general Čerenkov processes. Using a simple model and taking into account symmetry considerations, we identify the leaky modes that are important for the $\chi^{(2)}$-processes in the structures that we investigated.**

I. Introduction

THE interest in $\chi^{(2)}$-materials and related nonlinear wave-propagation effects has been driven for a long time by potential applications in efficient blue-light generation by Second Harmonic Generation (SHG) and electro-optical switching [1]. In addition, recent advances in $\chi^{(2)}$-materials allow for large nonlinear phase-shifts of the fundamental beam by the cascading of second-order effects [2]. This approach offers possibilities for tackling problems which have been traditionally thought to need third-order nonlinearities e.g., all optical switching [3].

From a practical point of view, the interest in SHG has been dominated by guided mode—guided mode interactions (here referred to as type A interactions) rather than by guided mode—radiation mode (type B) interactions (also called Čerenkov radiation) since the latter cause problems for the collection of the SH light as well as for analytical investigations. Initial papers on cascading [4] naturally focused on type A interactions since these could easily be analyzed by Coupled Mode Analysis (CMA). One of the remarkable results of the CMA of second-order cascaded processes is that both the magnitude and sign of the nonlinear phase-shifts can be tailored by choosing appropriate wavevector mismatches [4]. In the case of type B interactions, analytical relations are far more difficult to obtain due to the problems associated with the normalization of radiation modes and, thus, expressions for the nonlinear coupling coefficients are derived more difficult.

Manuscript received September 7, 1995. This work was supported by AFOSR and NSF. The research of G. J. M. Krijnen has been made possible by a fellowship of the Royal Netherlands Academy of Arts and Sciences.

G. J. M. Krijnen, H. J. W. M. Hoekstra, and P. V. Lambeck are with the Lightwave Devices Group, MESA Institute, University of Twente, P.O. Box 217, 7500 AE Enschede, The Netherlands.

W. Torruellas and G. I. Stegeman are with CREOL, University of Central Florida, 12424 Research Parkway, Suite 400, Orlando, Florida 32826 USA.

Publisher Item Identifier S 0018-9197(96)02557-2.

Čerenkov SHG has been previously treated by a number of authors [5]–[9]. The emphasis has been solely on the problem of calculating the SHG efficiency as a function of waveguide and material parameters, and there are no existing treatments of the nonlinear phase shift for this geometry. In most cases, the Čerenkov "cross-section" has been evaluated for a number of waveguide geometries under the assumption of steady-state SHG, primarily with CMA [10]. This is valid in the low depletion regime and far from the input facet where strong SHG can occur in a transition region before steady state is achieved [11]. Maxima in the SHG efficiency have been predicted as a function of parameters such as the waveguide width, index, etc. Although their exact nature has not been elucidated, such oscillations have been attributed to some form of resonances in the SHG signal across the waveguide core [12]. Depletion of the fundamental with propagation distance has been calculated by Suhara *et al.* [13] using a CMA approach, predicting a logarithmic behavior for strong fundamental depletion. Finally, BPM has been applied previously to this problem by Hayata *et al.* [14], [15], where the variation in the cross-section with waveguide, etc. parameters were investigated.

In this paper, we will describe a widely applicable method of analyses: the SHG Beam Propagation Method (SHG-BPM). This method is an extension of normal BPM's and offers a general approach to dealing with waves rather than with modes. The method circumvents the problems associated with depletion and nonnormalizable radiation modes encountered in coupled mode approaches. Using the SHG-BPM, we investigate the SHG efficiencies and nonlinear phase-shifts of both type A and type B interactions, and we also take into account the nontrivial case $n_c^{2\omega} < N_{\text{eff}}^{\omega}$ (where $n_c^{2\omega}$ is the core refractive index and N_{eff}^{ω} the guided wave effective index). We will first establish many of the recurring characteristics of these processes numerically and then interpret them physically.

Our analysis shows that SHG efficiencies can be strongly enhanced over general Čerenkov radiation near wavevector-matching with leaky modes. We find that large phase-shifts ($>\pi/2$) and almost complete conversion (97%) are possible with small input powers and short interaction lengths ($\approx$4 mm).

II. Numerical Method

For the numerical method employed in this paper, which we will refer to as SHG-BPM, we assume two-dimensional geometries with the x- and z-axes normal and parallel to the propagation direction, respectively (an extension to three-

dimensional geometries is straightforward). Inserting the nonlinear polarization [16] into the wave-equation using $\chi^{(2)}(-2\omega;\omega,\omega) = \chi^{(2)}(-\omega;2\omega,-\omega) \equiv \chi^{(2)}$, applying the Slowly Varying Envelope Approximation (SVEA) and discretizing the fields in the transverse (x-) direction, the propagation equations become

$$j\frac{\partial\bar{\psi}_f}{\partial z} = \mathbf{M}_f\bar{\psi}_f + \frac{1}{2n_0k_0}\frac{\partial^2\bar{\psi}_f}{\partial z^2} + \frac{k_0\chi^{(2)}}{n_0} \cdot \mathrm{col}[\psi_f^{i*}\psi_s^i,\cdots,\psi_f^{m*}\psi_s^m] \tag{1a}$$

$$j\frac{\partial\bar{\psi}_s}{\partial z} = \mathbf{M}_s\bar{\psi}_s + \frac{1}{4n_0k_0}\frac{\partial^2\bar{\psi}_s}{\partial z^2} + \frac{k_0\chi^{(2)}}{n_0}\bar{\psi}_f^2. \tag{1b}$$

In (1), the subscripts f and s refer to the fields at ω and 2ω, respectively, k_0 is ω/c, n_0 is a suitable background refractive index, $\bar{\psi}_f$, $\bar{\psi}_s$ are vectors representing the discretized field envelopes along the x-direction, and $\mathbf{M}_s$ and $\mathbf{M}_f$ are tri-diagonal discretization matrices. The equations are solved using a split-step approach; the first two linear operators are handled by an Enhanced Finite Difference Beam Propagation Method (EFDBPM) [17] whereas the third operator, which is given by the coupled differential equations

$$\begin{aligned} j\frac{\partial\psi_f^i}{\partial z} &= \alpha\psi_f^{i*}\psi_s^i \\ j\frac{\partial\psi_s^i}{\partial z} &= \alpha\psi_f^i\psi_f^i \end{aligned} \qquad \alpha = \frac{k_0\chi^{(2)}}{n_0}, \quad i\in(0,m) \tag{2}$$

is solved pointwise for all m discretization points and for each propagation step Δz. For integration over small distances Δz in which $|\psi_f^i|$ can be assumed to be a constant, (2) has eigenvalues $\pm\alpha|\psi_f^i|$. The corresponding eigenvectors are

$$\begin{bmatrix}\psi_f^i\\ \psi_s^i\end{bmatrix}_1 = \frac{1}{\sqrt{2}}\begin{bmatrix}e^{-j\phi}\\ 1\end{bmatrix} \quad \text{and} \quad \begin{bmatrix}\psi_f^i\\ \psi_s^i\end{bmatrix}_2 = \frac{1}{\sqrt{2}}\begin{bmatrix}e^{-j\phi}\\ -1\end{bmatrix}, \tag{3}$$

where ϕ is the phase of ψ_f^i, i.e., $\psi_f^i \equiv |\psi_f^i|e^{j\phi}$. The numerical accuracy of the solution of (2) is increased by integrating (2) in three steps for each step Δz of the EFDBPM. The accuracy of each of these three steps on its turn is improved by first predicting the values of $\psi_f^i(z+\Delta z)$ and using $\psi_f^i = 0.5(\psi_f^i(z)+\psi_f^i(z+\Delta z))$ in (3) (e.g., second-order Runge-Kutta integration, [18]). In principle, other BPM's can be used as well. Although (1) will be different, (2) can be solved in the same way. Here, the EFDBPM was chosen because of the high accuracy with which it calculates propagation constants [17].

To keep calculation times reasonable and the accuracy of the simulations independent of the window size, we used transparent boundary conditions [19]. This is extremely important since at 2ω we are dealing primarily with radiation modes. In all the SHG-BPM calculations, the stepsizes in propagation (z-) and lateral (x-) directions are fixed at 1 and $\approx$0.1 μm, respectively. In order to evaluate the power in the fields at ω and 2ω, we calculate the overlap of the field at ω with the field of the launched guided mode. Since there is no radiative loss at ω for a straight, linear waveguide, the difference between the launched power and the power in the guided mode at some propagation distance z is equal to the power that has been converted to 2ω up to that position.

III. Numerical Studies

A. Structures

As an example, we studied a slab-waveguide, with cladding refractive index $n_{\mathrm{cl}}^{\omega} = 1.6875$, a 5 μm wide core with $n_c^{\omega} = 1.6992$ and a $\chi^{(2)}$ of 54 pm/V. The fundamental wavelength (λ_f) was set at 1.32 μm. The effective indices of the fundamental and first-order mode at ω were $\mathrm{TE}_0^{\omega} = 1.696\,72$ and $\mathrm{TE}_1^{\omega} = 1.690\,23$, respectively. We investigated three different cases in which the refractive indices at ω are fixed whereas the indices at 2ω are varied systematically (see Fig. 1). In Case I (see Fig. 1, top), the refractive indices are chosen in order to have guided modes at 2ω, and a TE_0^{ω} mode is launched. This case shows a (classical) type A interaction, which can also be modeled by CMA and therefore enables us to check the accuracy of the SHG-BPM code. In Case II (see Fig. 1, middle), again the TE_0^{ω} mode is launched. However, the refractive index of the core at 2ω ($n_c^{2\omega}$) is varied around the value of the effective refractive index of the TE_0^{ω} mode whereas the refractive index of the cladding at 2ω ($n_{\mathrm{cl}}^{2\omega}$) is fixed and higher than ($n_c^{2\omega}$) so that no guided modes exist at 2ω. Case III (see Fig. 1, bottom) is similar to Case II but differs in so far that the TE_1^{ω} mode is launched whereas $n_c^{2\omega}$ is varied around the value of the effective refractive index of the TE_1^{ω} mode. The three different cases are summarized in Table I.

Case I: This case serves as a validity-check of our algorithm by comparing the results obtained by the SHG-BPM calculations to those of CMA. To this end, the index-distribution for this structure is chosen such that there exist guided modes at 2ω. The refractive indices of the structure are shown in Fig. 1 (top) and Table I. Moreover, this case is used as a reference for the calculations on type B interactions of Cases II and III, which are the actual topic of this paper.

In a series of calculations, the index profile at 2ω was shifted so that a variety of phase-matching conditions was encountered for varying Δn. Fig. 2 shows an example of the SHG-BPM results for a Δn value for which the TE_0^{ω} and $\mathrm{TE}_0^{2\omega}$ modes are almost phase-matched (coherence length $\approx$ 1100 μm, $\Delta N_{\mathrm{eff}} = N_{\mathrm{eff}}^{2\omega} - N_{\mathrm{eff}}^{\omega} \approx 6\cdot 10^{-4}$). Fig. 3 (top) shows the transmission of the fundamental beam as a function of Δn at a propagation distance of 1.0 mm. The dashed vertical lines in Fig. 3 indicate the positions for which the TE_0^{ω}-mode is phase-matched to one of the $\mathrm{TE}^{2\omega}$ modes. Narrow minima in the fundamental throughput are obtained at phase-matching to guided modes at 2ω provided that the nonlinear overlap integral

$$C_{\mathrm{nl}} = \frac{\varepsilon_0\omega}{2}\int_{x=-\infty}^{+\infty}\chi^{(2)}(x)E_j^{2\omega}(x)\left[E_i^{\omega *}(x)\right]^2 dx \tag{4}$$

is nonzero for these modes. For the symmetrical structure studied, this was the case for the $\mathrm{TE}_0^{2\omega}$ ($C_{\mathrm{nl}} = 1.395$) and $\mathrm{TE}_2^{2\omega}$ ($C_{\mathrm{nl}} = -0.121$) modes ($\Delta n = -6.87\cdot 10^{-3}$ and $8.28\cdot 10^{-5}$, respectively). The curves show the characteristic sinc^2 appearance with sharp minima at phase-matching. Fig. 3 (top) clearly shows that the SHG-BPM calculations are very accurately reproduced by CMA. Note that in the

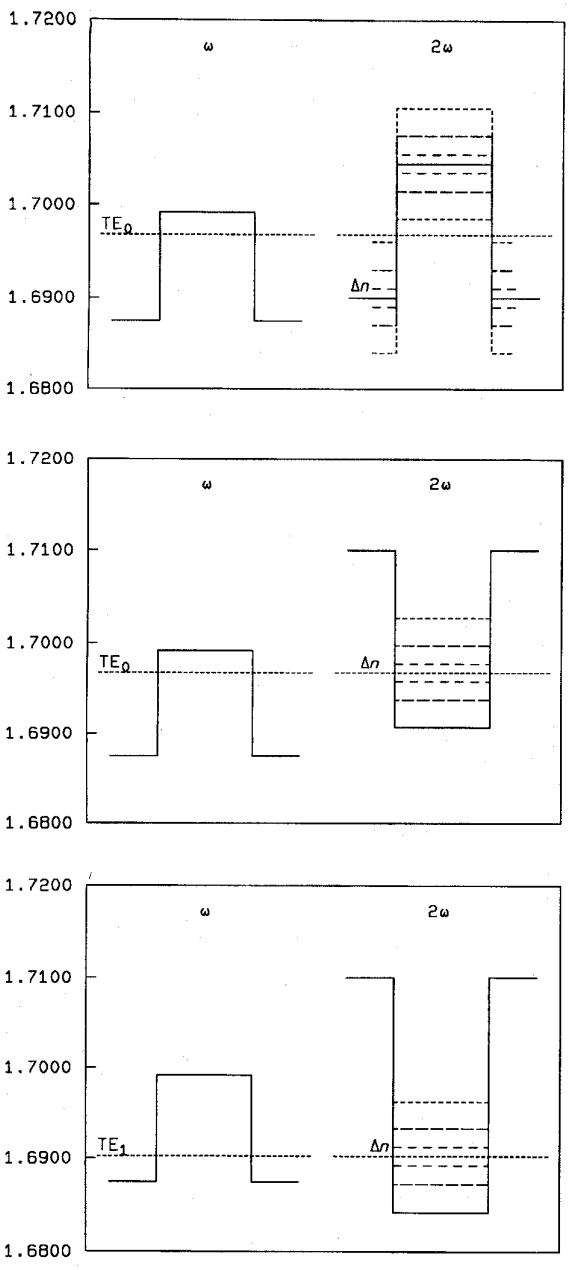

Fig. 1. Graphical illustration of the structures used in Case I (top), Case II (middle), Case III (bottom). The dotted horizontal lines denoted TE_0 and TE_1, indicate the effective refractive index levels of the guided modes at ω. The dashed lines in the right parts of the graphs illustrate the parts of the refractive index profiles that are varied in the calculations.

SHG-BPM calculations one does not have to include any specific information about the modes because this is taken into account automatically as evidenced by the shallow minimum at $\Delta n = 8.28 \cdot 10^{-5}$ corresponding to phase-matching between the TE_0^{ω} and $TE_2^{2\omega}$ modes. Interesting in Fig. 3 (top) is also the shallow minimum at $\Delta n \approx 10 \cdot 10^{-3}$ which cannot be accounted for by phase-matching to any guided mode since at this Δn the structure is already in the Čerenkov-regime. Fig. 3 (bottom) shows the nonlinear phase-shift of the fundamental at a propagation distance of 4.3 mm versus Δn. Again, the

TABLE I
DATA OF THE CASES STUDIED IN THIS PAPER

Case	Width/μm	n_c^{ω}	n_{cl}^{ω}	$n_c^{2\omega}$	$n_{cl}^{2\omega}$	Input
I	5	1.69920	1.68750	1.70450 + Δn	1.69000 + Δn	TE_0^{ω}, 8.5 MW/m
II	5	1.69920	1.68750	1.69672 + Δn	1.71000	TE_0^{ω}, 8.5 MW/m
III	5	1.69920	1.68750	1.69023 + Δn	1.71000	TE_1^{ω}, 8.5 MW/m

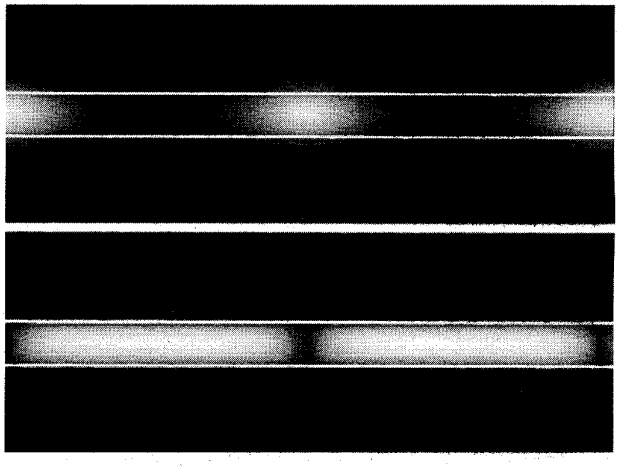

Fig. 2. Example of results obtained with the SHG-BPM for Case I. $\Delta n = -6.875 \cdot 10^{-3}$ (close to phase matching). Upper graph: Fundamental field. Lower graph: second harmonic field. The images correspond to an area of 25 μm $*$ 4300 μm. The input power is 8.5 MW/m.

results of the CMA and the SHG-BPM calculations agree very well with each other. From this graph, it is very clear that the nonlinear phase-shifts are dominated by the resonance of the $TE_0^{\omega} - TE_0^{2\omega}$ interaction, a result which can be well understood from an approximate CMA analysis of the nonlinear phase-shifts which predicts a quadratic dependence on the nonlinear coupling constants [4].

Fig. 4 top shows the transmission of the TE_0^{ω} mode versus P_{in}^{ω} and propagation distance (z) for $\Delta n = -7.0 \cdot 10^{-3}$ (close to the deep minimum at $\Delta n = -6.87 \cdot 10^{-3}$ in Fig. 3 (top)) as calculated by the SHG-BPM. At low power (1 MW/m), there is already an appreciable amount of conversion. When the power is increased, this conversion becomes more complete, but at the same time, the coherence length shortens causing an increasing number of oscillations within a fixed length. This means that it is difficult to obtain complete conversion since the amount of SHG depends on both the length of the structure as well as the input power. Fig. 4 (bottom) displays the nonlinear phase-shift due to cascading as a function of P_{in}^{ω} and propagation distance. It shows that at fixed Δn the nonlinear phase-shift per oscillation of the power between the fields at ω and 2ω is fixed giving the graph its staircase-like appearance. However, as the input power increases, the number of oscillations increases and thereby the total nonlinear phase-shift at the output. These SHG-BPM results are consistent with CMA analyses of type A interactions published in [4] as well as with CMA calculations carried out for this structure (but not shown here).

Case II: Structure II resembles the waveguide properties of a DAN crystal-core fiber for which large nonlinear phase-shifts

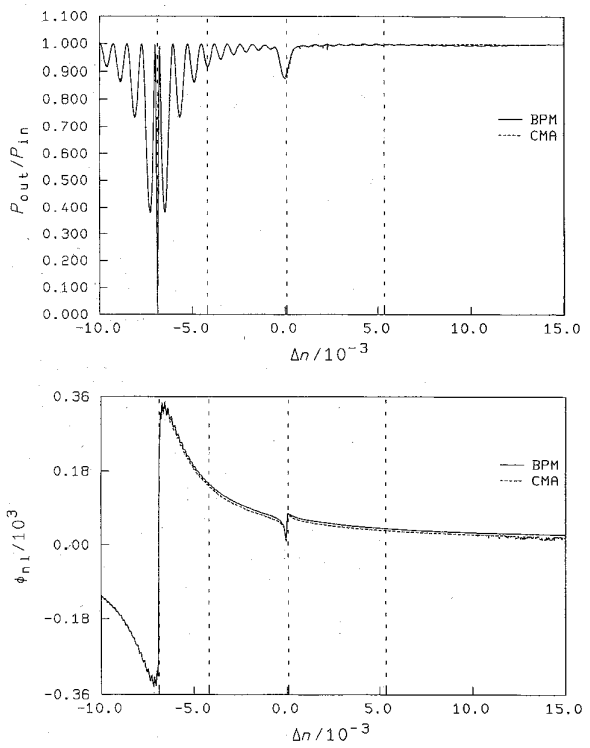

Fig. 3. Power (top) and phase (bottom) versus detuning Δn for the TE_0^ω mode in Case I. The dashed vertical lines indicate the Δn values for which the launched mode is wavevector-matched to one of the guided modes at 2ω.

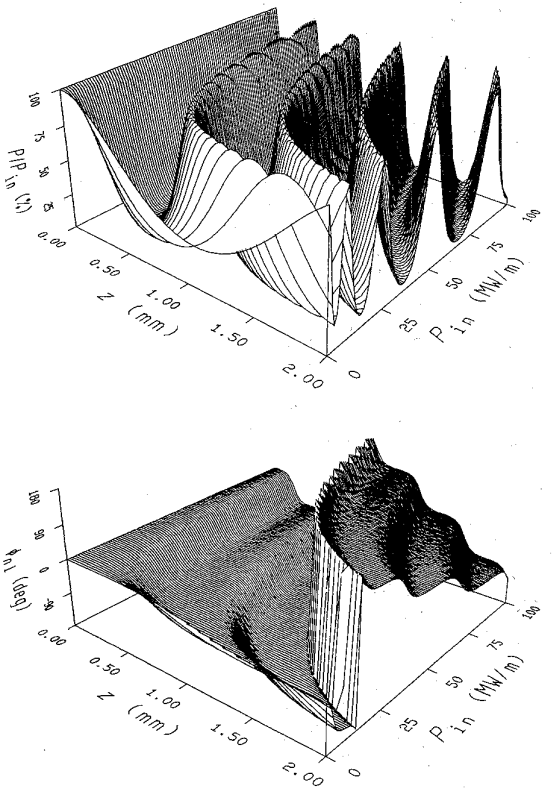

Fig. 4. Fraction of power in the TE_0^ω mode (top) and the unwrapped (i.e., modulo 180°) nonlinear phase-shifts (bottom) as a function of input power and propagation distance for Case I. $\Delta n = -7.0 \cdot 10^{-3}$. Note that only the first 2 mm of propagation is shown.

have been measured recently [20]. In this case, the core index $n_c^{2\omega}$, which is not well-known experimentally, was varied in a series of calculations. In all of the simulations, initially (i.e., at small propagation coordinate) a strong generation of SHG, followed by a steady outflow of power at 2ω is observed, and simultaneously, the TE_0^ω-mode is quickly depleted, changing over to exponential decay at longer distances. This is illustrated in Fig. 5 which is obtained for $\Delta n \equiv n_c^{2\omega} - N_{TE_0}^\omega = 1 \cdot 10^{-3}$. In some simulations, the initial fields showed oscillations between apparently guided fields at ω and 2ω. However, these oscillations tend to damp out rather quickly. Fig. 5 (bottom) shows the transverse profile of the fields at ω (left) and 2ω (right) after 4.3 mm of propagation, plotted in logarithmic form. Since strong interaction with the field at 2ω only takes place in the first 1–2 mm, the field at ω decreases linearly in the cladding, neatly corresponding to a guided mode. The field profile at 2ω will be discussed below.

The depletion and phase shift of the TE_0^ω mode at a propagation distance of 4.3 mm, corresponding to the length of the DAN crystal-core fiber in [20], are shown as a function of Δn for $P_{in}^\omega = 8.5$ MW/m in Fig. 6 (top) and (bottom), respectively. Clearly, the depletion (i.e., SHG conversion-efficiency) and nonlinear phase shift are strongly dependent on Δn and, moreover, the sign of the nonlinear phase shift can be positive or negative, depending on Δn. These results are very similar to the nonlinear phase shifts obtained for type A interactions near phase-matching. Note that zero phase-shift and maximum depletion do not coincide with $\Delta n = 0$ but are shifted to positive Δn ($\approx 1 \cdot 10^{-3}$), a result which we confirmed to depend neither on the accuracy of the SHG-BPM calculations nor on P_{in}^ω (by calculations at smaller P_{in}^ω not shown here).

In order to investigate the dependence of the depletion and nonlinear phase shift on P_{in}^ω, a series of calculations with increasing input power was performed at $\Delta n = 2.5 \cdot 10^{-3}$. This is where the nonlinear phase-shift is maximum in Fig. 6 (bottom). Fig. 7 (top) shows the fraction of power remaining in the TE_0^ω mode as a function of P_{in}^ω and propagation distance (z-). At low power, the depletion (i.e., SHG-conversion) is modest. However, on increasing the power, the coupling between the fields at ω and 2ω increases (like for a type A interaction) and the conversion becomes more complete leading to almost entire depletion (conversion) of the TE_0^ω mode at longer propagation distances. At the highest input powers, there is a (damped) oscillation discernible in the first few hundred microns. This oscillation corresponds to forward and backward coupling between the fields at the two wavelengths. This result is not expected on the basis of the general notion that Čerenkov radiation is automatically phase-matched. Fig. 7 (bottom) shows the nonlinear phase-shift by cascading as a function of P_{in}^ω and propagation distance. Clearly, the nonlinear phase-shift increases with both P_{in}^ω and propagation distance. However, combining the results displayed in Fig. 7 (top) and (bottom), it appears that for this value of Δn large nonlinear phase-shifts can only be obtained

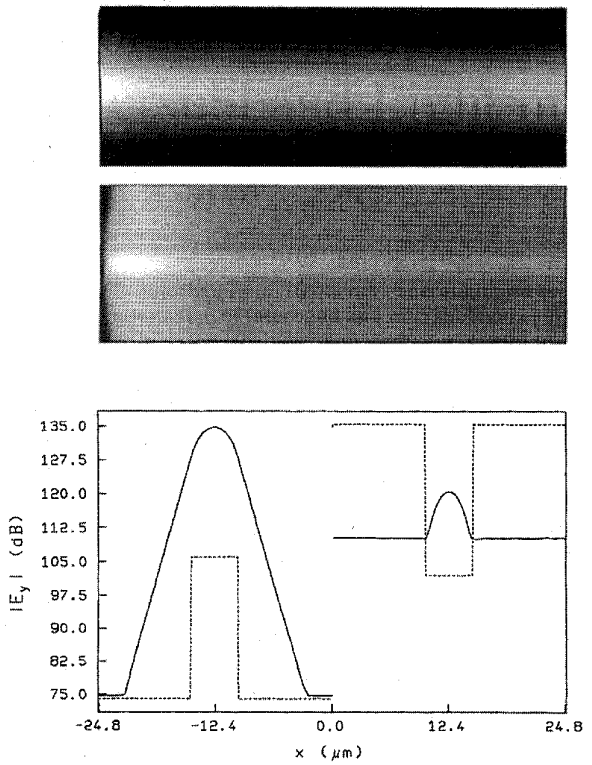

Fig. 5. Example of results obtained with the SHG-BPM for Case II and $\Delta n = 1 \cdot 10^{-3}$. Top: Intensity profiles at ω (upper part) and 2ω (lower part). The profiles are plotted on a 60 dB scale, and the figures correspond to an area of 25 μm $*$ 4.3 mm. Bottom: Field profile at the output of the structure on a logarithmic scale. The field profiles at ω (left) and 2ω (right) are both shown. The dotted line shows the index profiles.

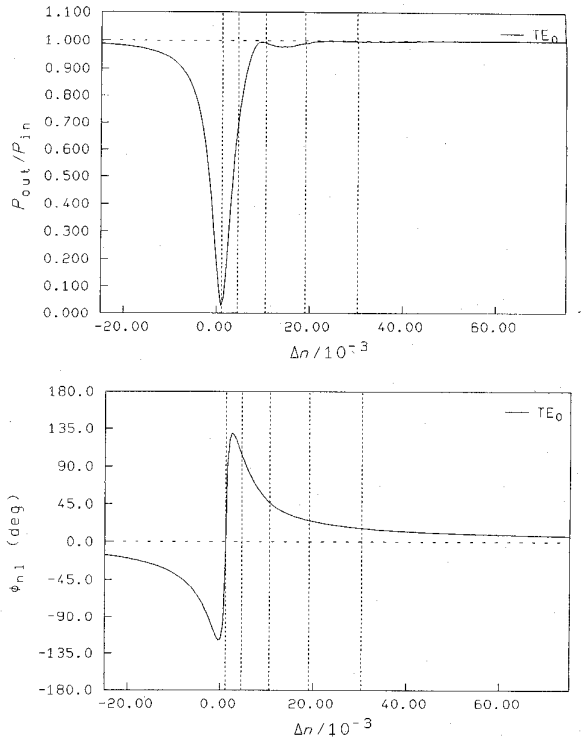

Fig. 6. Power (top) and nonlinear phase shift (bottom) versus detuning Δn for Case II. The dotted vertical lines indicate the effective index levels of leaky modes.

at the expense of losing considerable power from the TE_0^ω mode to the 2ω field, thereby continuously slowing down the rate of change of the nonlinear phase-shift.

A closer examination of Fig. 6 shows that large nonlinear phase-shifts in the Čerenkov regime are not always accompanied by large fundamental depletion. At $\Delta n = 9.5 \cdot 10^{-3}$, the transmission at 4.3 mm is >99% while a nonlinear phase-shift of 53° is still obtained. Calculations with varying input power for this Δn value are shown in Fig. 8. The upper graph shows the transmission of the TE_0^ω mode versus power and propagation distance. Clearly, even at the highest input power (100 MW/m) and at the longest calculated propagation distance (4.3 mm), the depletion is less than 10%. However, Fig. 8 (bottom) shows that the nonlinear phase-shift is as high as ≈540°. Note that this is larger than the largest nonlinear phase-shift obtained with $\Delta n = 2.5 \cdot 10^{-3}$, despite the fact that this latter value produced the largest nonlinear phase-shift at $P_{\text{in}}^\omega = 8.5$ MW/m. Fig. 8 (bottom) also shows an approximately linear dependence of the nonlinear phase-shift on both the input power and propagation length. This is important since it means that large nonlinear phase-shifts can be obtained for long propagation lengths. This is clearly not the case when most of the input power is depleted. Furthermore, it is beneficial for many applications in which a linear dependence of the nonlinear phase-shift with input power is desirable. We believe that this fortunate combination of low depletion and a nonlinear phase-shift that is proportional to the input power and propagation length can occur only whenever the propagation constant of the launched mode lies between two phase-matching resonances.

In conclusion, we observed nonlinear phase-shifts and depletion in the Čerenkov regime which show a behavior as function of $\Delta n = n_c^{2\omega} - N_{\text{TE}_0}^\omega$ that strongly resembles regular type A interactions. Depending on Δn, these interactions can produce almost complete conversion of the fundamental beam into (unguided) SHG or they can produce large nonlinear phase-shifts that are nearly linear with input power and propagation length while showing very low depletion.

Case III: The calculations performed for Case III were very similar to those for Case II. The principal difference was that the TE_1^ω-mode was launched instead of the TE_0^ω-mode. Fig. 9 (top), obtained for $\Delta n = 10 \cdot 10^{-3}$, shows an example of the SHG-BPM results. At this value of Δn, there is considerable conversion of power to the 2ω field. However, the 2ω field profile differs strongly from the one displayed in Fig. 5 which was obtained in Case II and, moreover, the field is much smaller. This is very well shown in Fig. 9 (bottom) where the fundamental (left) and SHG (right) fields are shown. It should be emphasised though, that SHG field profiles similar to the one shown in Fig. 5 are obtained for Δn-values of about $1 \cdot 10^{-3}$.

The nonlinear phase shift and depletion of the TE_1^ω mode at the output of the structure as a function of $\Delta n \equiv n_c^{2\omega} - N_{\text{TE}_1}^\omega$ are shown for $P_{\text{in}}^\omega = 8.5$ MW/m in Fig. 10 (top) and (bottom), respectively. Obviously, like in Case II, the nonlinear phase

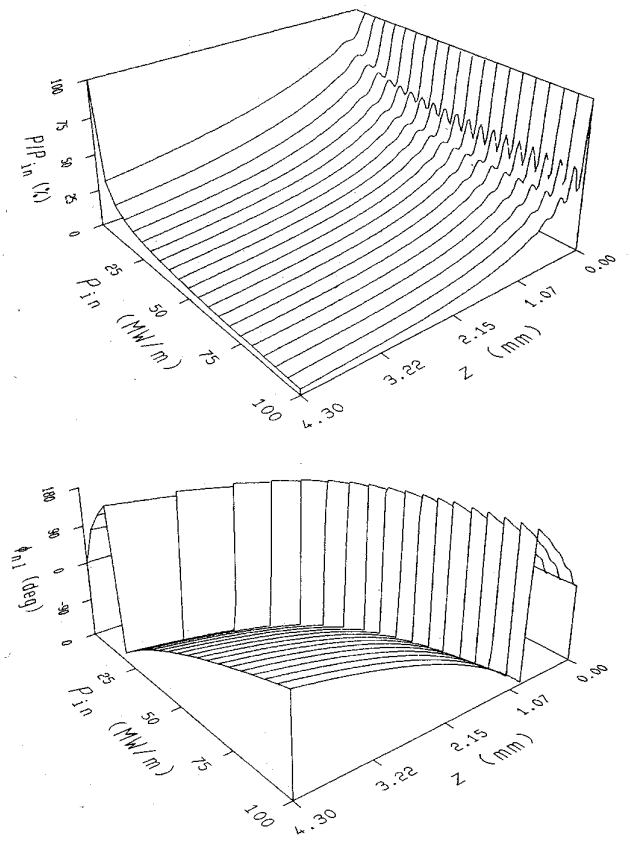

Fig. 7. Fraction of power in the TE_0^ω mode (top) and the unwrapped nonlinear phase-shifts (bottom) as a function of input power (P_{in}^ω) and propagation distance (z-coordinate) for Case II. $\Delta n = 2.5 \cdot 10^{-3}$.

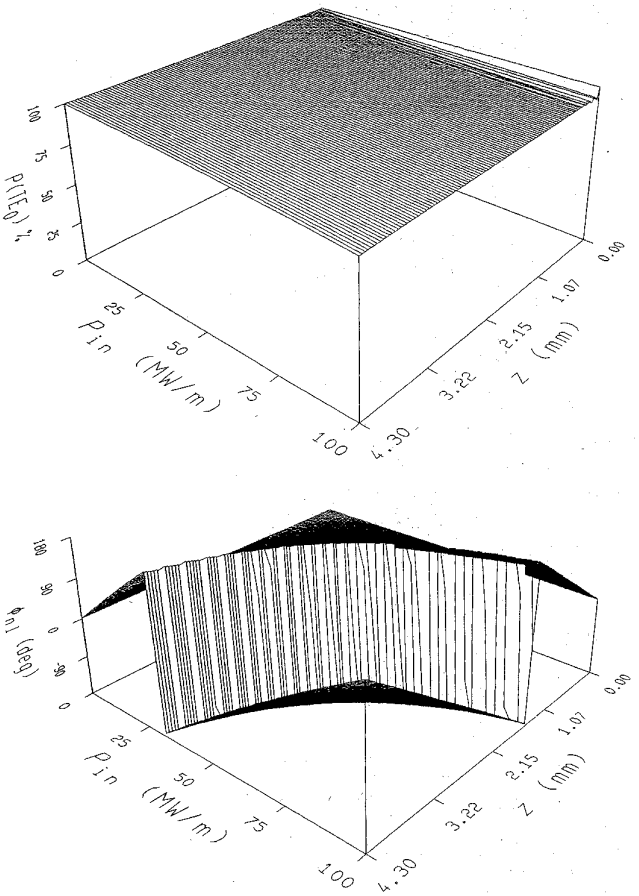

Fig. 8. Fraction of power in the TE_0^ω mode (top) and the unwrapped nonlinear phase-shifts (bottom) as a function of input power (P_{in}^ω) and propagation distance (z-coordinate) for Case II. $\Delta n = 9.5 \cdot 10^{-3}$.

shift and depletion are strongly dependent on Δn. Fig. 10 (top) shows three distinct minima in the transmission curve (corresponding to three maximums in the SHG output) of the TE_1^ω mode at Δn-values of $1 \cdot 10^{-3}$ (32.3% transmission), $10 \cdot 10^{-3}$ (73.5%) and $32 \cdot 10^{-3}$ (98.7%). The deepest minimum obtained in this case is not as wide and deep as the one obtained for Case II at $\Delta n = 1 \cdot 10^{-3}$ (2.9% transmission) implying that SHG is less efficient. Dispersion in the nonlinear phase-shift, centred at two of the three minima was found, again very similar to the nonlinear phase-shifts obtained for type A interactions when tuning through phase-matching conditions.

IV. Analysis of Numerical Studies

The simulations of Cases II and III suggest that there exist certain phase-matching conditions in the Čerenkov regime that behave as if type A SHG (i.e., to guided modes at 2ω) takes place. This is evidenced by deep dips in the transmission and large nonlinear phase-shifts of the TE^ω modes. Since the radiation modes form a continuum, this discrete behavior is somewhat unexpected (although other authors [6]–[10], [13], [14] have shown similar maxima in the SHG power via Čerenkov processes, e.g., as a function of waveguide layer thickness). However, within the radiation modes there exist a class of discrete modes that have a relatively low propagation loss (as compared to radiation modes in general): the so-called leaky modes. The existence of these modes stems from the constructive interference of waves that are weakly bound by incomplete reflections at the parallel interfaces [21]. Due to the lack of total reflection, leaky modes have propagation losses causing them to have complex propagation constants. In order to determine whether leaky modes can play an important role in the SHG processes studied, we calculated the effective indices and field profiles of these modes for the structures that were considered here. Since the field profiles of these leaky modes extend to infinity, they cannot be normalized, but their basic shapes can be calculated easily, and their symmetry properties determined. These field profiles are shown in Fig. 11. Note that, although the modulus of the profiles is symmetrical for all of the four modes displayed, the actual field profile is not symmetric for all modes; the first- and the third-order mode are symmetrical, but the second and the fourth are anti-symmetric. From these symmetry considerations, some important conclusions can be drawn for the nonlinear overlap integrals (C_{nl}) which are proportional to

$$C_{\text{nl}} \propto \int_{x=-\infty}^{+\infty} \chi^{(2)}(x) E_j^{2\omega}(x) \left[E_i^{\omega *}(x)\right]^2 dx, \qquad (5)$$

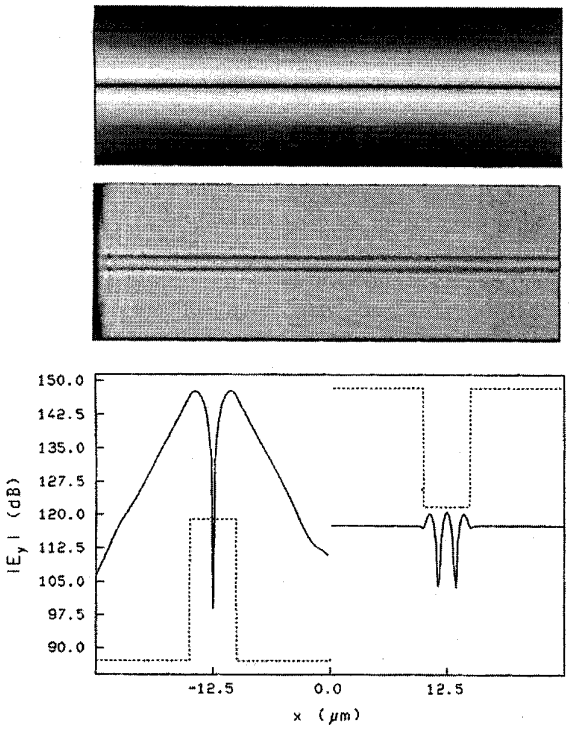

Fig. 9. Example of results obtained with the SHG-BPM for Case III and $\Delta n = 1 \cdot 10^{-2}$. Top: Intensity profiles at ω (upper part) and 2ω (lower part). The profiles are plotted on a 60 dB scale, and the figures correspond to an area of 25 μm $*$ 4.3 mm. Bottom: Field profile at the output of the structure on a logarithmic scale. The field profiles at both ω (left) and 2ω (right) are shown. The dotted lines show the index profiles.

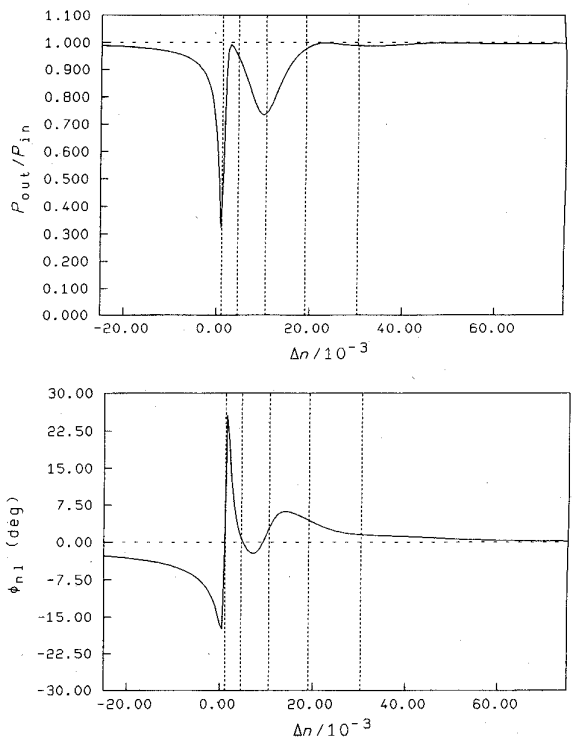

Fig. 10. Power (top) and nonlinear phase shift (bottom) versus detuning Δn for Case III. The dotted vertical lines indicate the effective index levels of leaky modes.

TABLE II
PROPERTIES OF THE LEAKY MODES OF CASES II AND III

Mode Order	N_{eff}	Loss dB/cm	Symmetry
1	1.696723	400	Symmetric
2	1.693242	1558	Anti-symmetric
3	1.687276	3368	Symmetric
4	1.678713	5704	Anti-symmetric
5	1.667476	8471	Symmetric

where $E_i^{\omega}(x)$ and $E_j^{2\omega}(x)$ are the fieldprofiles of the ith guided mode at ω and the jth leaky mode at 2ω, respectively. Since the structures investigated have symmetrical index profiles, the guided modes are either symmetrical or anti-symmetrical. Hence, the square of the field-profile in (5) will always be symmetrical. This means that the overlap of the guided modes with any of the antisymmetric leaky modes will always be zero ruling out SHG for these modes. The properties of the five lowest order leaky modes are summarized in Table II. Note that the Δn values for which wavevector matching to leaky modes occurs, are already indicated in Figs. 6 and 10 by dotted vertical lines.

Now combining the symmetry argument with phase-matching constraints, the results in Fig. 6 can be put into perspective. Due to the shape of the TE_0^{ω} field profile, the overlap with the second and fourth leaky mode will be zero. However, the overlap with the first and third leaky modes is nonzero, with the overlap with the first leaky mode being much larger than the overlap with the third. This explains the large depletion at wavevector-matching with the first leaky mode and the dominance of this resonance in the nonlinear phase-shift (Fig. 6 (bottom)). The similarity of the field profile at 2ω in Case II (Fig. 5 (bottom)) with the first leaky mode (Fig. 11 (left, top)) is consistent with this interpretation. Similar remarks can be made for Case III. The major difference here is that the nonlinear overlap of the TE_1^{ω} mode with the first and third leaky mode at 2ω is much smaller, and the two nonlinear coupling constants are closer in value. Hence, at the fixed power of 8.5 MW/m, the TE_1^{ω} mode will experience less loss (i.e., the SHG efficiency is smaller) than the TE_0^{ω} mode resulting in a sharper and shallower dip. Additionally, the nonlinear phase-shifts are less dominated by the resonance of the first leaky mode (especially well illustrated in the nonlinear phase shift, Fig. 10 (bottom)). Again, the mode profile at 2ω (Fig. 9 (bottom, right)) shows good similarity with the calculated leaky mode (Fig. 11 (left, bottom)).

The observed resonances for Case I are also consistent with the proposed scheme as can be seen from Fig. 12 which displays the logarithm of the generated SHG versus Δn for a propagation length of 2 mm as calculated by the SHG-BPM. In this case, the nonlinear overlap integrals of the TE_0^{ω} mode with the guided modes at 2ω are much larger than the overlap with the leaky modes at 2ω. Hence, in this case, the nonlinear response is dominated by type A interactions with

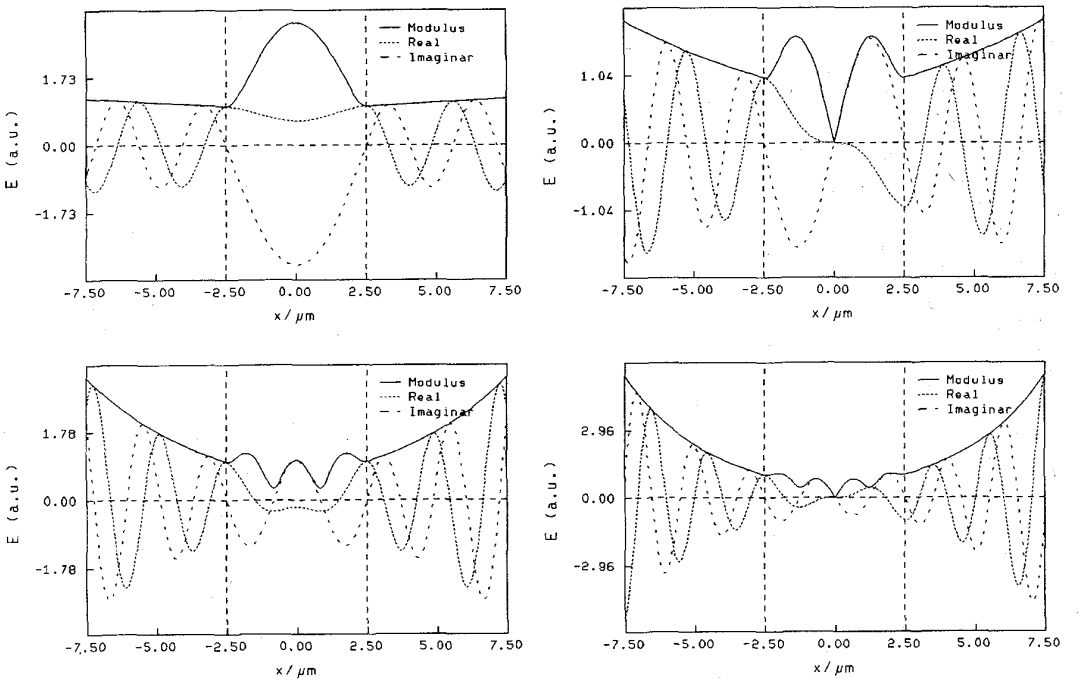

Fig. 11. Field profiles of the first four leaky modes at 2ω. Note the symmetry of modes 1 and 3 (left) and the asymmetry of modes 2 and 4 (right).

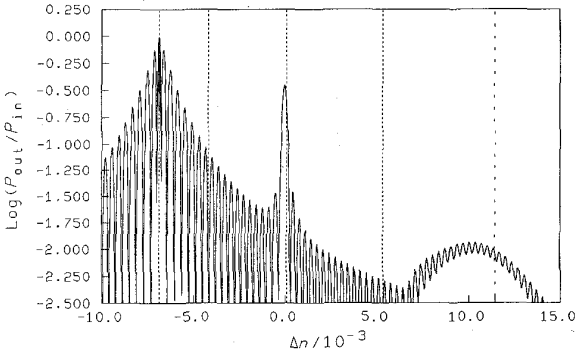

Fig. 12. Generated SHG on a logarithmic scale for Case I as calculated by the SHG-BPM. The dotted and dashed lines show the positions where the TE_0^{ω} mode is phase-matched to, respectively, guided and leaky $TE^{2\omega}$ modes.

the exception of a small peak near the position of the first leaky mode ($\Delta n = 11.43 \cdot 10^{-3}$). This leaky mode has four lobes causing the overlap with the TE_0^{ω} mode to be fairly small resulting in very small SHG. We speculate that the small shift of the SHG peak away from the position of the leaky mode is due to the nonlinear detuning caused by the much stronger resonance of the $TE_0^{\omega}-TE_0^{2\omega}$ interaction.

With respect to the growth of the second harmonic waves with propagation distance, the SHG-BPM calculations show that at $z = 0$, many (radiation) modes are excited (see e.g., Figs. 5 and 9). However, since most of these modes are not wavevector-matched and since the flow of power out of the core is very large (i.e., very high losses), there is no considerable buildup in these radiation modes. Therefore, these modes only cause some loss of power in the initial few hundred wavelengths of propagation after which coherent conversion processes become dominant. The lower order leaky modes with relatively low attenuation and large nonlinear overlaps qualify especially well to take part in these coherent processes.

We emphasize that at the power levels at which the simulations were done, virtually no SHG was found to either a guided or a leaky mode when the systems were far from phase-matching. In our opinion, this means that phase matching to leaky modes is of prime importance for SHG in the Čerenkov regime, enhancing the SHG efficiency by orders of magnitude.

V. Discussion

Our calculations have shown that, for comparable structures, type A interactions exhibit I) sharper resonances, II) stronger SHG, and III) larger maximum nonlinear phase-shifts than type B interactions. This basically means that type A interactions qualify better for both SHG and nonlinear phase-shift applications, provided that one can precisely control the waveguide structure and the experimental conditions. However, type B interactions do have some important advantages:

I) Due to the large losses of the leaky modes, type B interactions are far less critical to phase-matching constraints. The benefits are that small deviations in waveguide structure, device length, input power, and wavelength do not dramatically change the fundamental and harmonic wave outputs. Thus, although SHG may be less efficient for type B than for type A, it can still be competitive since the conversion of fundamental to harmonic waves increases monotonically with propagation distance enabling large conversion at larger device lengths. Therefore, type B interactions are preferable for SHG provided

it is possible to satisfactorily collect the light emitted via the leaky modes at 2ω.

II) Our calculations have shown that for carefully chosen phase-mismatch conditions, the nonlinear phase-shifts are proportional to input power and propagation length concurrent with very small fundamental power conversion to 2ω. We note that this is a very desirable condition for devices in which one tries to exploit nonlinear phase-shifts.

Of course, the potential of type B interactions can only be realized when appropriate materials, e.g., materials with very dissimilar dispersion, large birefringence, or anomalous dispersion, are available. It has recently been shown that DAN [20], [22] and doped PMMA [23] are in principle such materials. Moreover, our calculations have shown (see Fig. 12) that one can utilize leaky modes even if the structure at 2ω is a guiding structure albeit that the nonlinear interaction with leaky modes is strongest when the number of guided modes is small (due to larger overlaps for lower order modes).

VI. Conclusion

In conclusion, we have described a method (SHGBPM) for evaluating the interaction of propagating fields in $\chi^{(2)}$-materials and devices. We have shown that the SHGBPM takes into account both the depletion and the nonlinear phase-shifts of the fundamental fields. We have employed the SHGBPM to investigate SHG and cascading in a range of waveguide geometries including the Čerenkov regime. Our calculations predict that the SHG conversion in this regime (Čerenkov) can be enhanced by orders of magnitude when there is wavevector-matching with leaky modes, resulting in near complete conversion of the fundamental beam into the second harmonic. As in the case of type A interactions, the nonlinear phase-shift changes sign when tuning through wavevector-matching. For some structures, the conversion of the fundamental beam can be quite low while still obtaining large nonlinear phase-shifts that are approximately proportional to input power and propagation length. Type B interactions seem especially useful for applications that require noncritical structures and working conditions.

Acknowledgment

The authors acknowledge the many fruitful discussions with Roland Schiek.

References

[1] "Compact blue-green lasers," in *OSA Tech. Dig. Series*, Santa Fe, NM, 1992.

[2] M. Sundheimer, C. Bosshard, E. Van Stryland, G. Stegeman, and J. D. Bierlein, "Large nonlinear phase modulation in quasi phase-matched KTP waveguides due to cascaded second order processes," *Opt. Lett.*, vol. 18, pp. 1397–1399, 1993.

[3] *Photonics in Switching*, J. E. Midwinter, Ed. London, England: Academic, 1993.

[4] G. Stegeman, M. Sheik-Bahae, E. van Stryland, and G. Assanto, "Large nonlinear phase shifts in second order nonlinear-optical processes," *Opt. Lett.*, vol. 18, pp. 13–15, 1993.

[5] K. Chikuma and S. Umegaki, "Characteristics of optical second-harmonic generation due to Čerenkov-radiation-type phase matching," *J. Opt. Soc. Am. B*, vol. 7, pp. 768–775, 1990.

[6] T. Onda and R. Ito, "Theory of optical second-harmonic generation in slab waveguides," *Jap. J. Appl. Phys.*, vol. 30, pp. 957–982, 1991.

[7] G. Leo, R. Drenten, and M. Jongerius, "Čherenkov second-harmonic generation in multilayer waveguide structures," *IEEE J. Quantum Electron.*, vol. 28, pp. 534–546, 1992.

[8] N. Hashizume, T. Kondo, T. Onda, N. Ogasawara, S. Umegaki, and R. Ito, "Theoretical analysis of Čerenkov-type optical second-harmonic generation in slab waveguides," *IEEE J. Quantum Electon.*, vol. 28, pp. 1798–1815, 1992.

[9] K. Chikuma and S. Umegaki, "Theory of optical second-harmonic generation in crystal-cored fibers based on phase matching of Čerenkov-type radiation," *J. Opt. Soc. Am. B*, vol. 9, pp. 1083–1092, 1992.

[10] H. Tamada, "Coupled-mode analysis of second harmonic generation in the form of Čerenkov radiation from a channel waveguide."

[11] G. J. M. Krijnen, W. Torruellas, G. I. Stegeman, P. V. Lambeck, and H. J. W. M. Hoekstra, "Nonlinear phase-shifts by cascading in the Čerenkov regime," in *Guided-Wave Optoelectronics: Device Characterization and Design*, T. Tamir, H. Bertoni, and G. Griffel, Eds. New York: Plenum, 1995.

[12] K. Hayata, T. Sugawara, and M. Koshiba, "Modal analysis of the second-harmonic electromagnetic field generated by the Čherenkov effect in optical waveguides," *IEEE J. Quantum Electron.*, vol. 26, pp. 123–134, 1990.

[13] T. Suhara, T. Morimoto, and H. Nishihara, "General coupled-mode analysis of Čerenkov-radiation-type second-harmonic generation in channel and fiber waveguides," *IEEE J. Quantum Electron.*, vol. 29, pp. 525–537, 1993.

[14] K. Hayata and M. Koshiba, "Numerical simulation of guided wave SHG light sources utilising Čerenkov radiation scheme," *Electron. Lett.*, vol. 25, pp. 376–378, 1989.

[15] K. Hayata and M. Koshiba, "Three-dimensional simulation of guided wave second harmonic generation in the form of coherent Čerenkov radiation," *Opt. Lett.*, vol. 16, pp. 1563–1565, 1991.

[16] A. Yariv and P. Yeh, *Optical Waves in Crystals*. New York: Wiley, 1984.

[17] H. J. W. M. Hoekstra, G. J. M. Krijnen, and P. V. Lambeck, "New formulation of the beam propagation method based on the slowly varying envelope approximation," *Opt. Commun.*, vol. 97, pp. 301–303, 1993.

[18] W. Press, B. Flannery, S. Teukolsky, and W. Vetterling, *Numerical Recipes*. Cambridge, UK: Cambridge Univ. Press, 1990, ch. 15.

[19] G. Hadley, "Transparent boundary conditions for beam propagation," *Opt. Lett.*, vol. 16, pp. 624–626, 1991.

[20] D. Kim, W. Torruellas, J. Kang, C. Bosshard, G. Stegeman, P. Vidakovic, J. Zyss, W. Moerner, R. Twieg, and G. Bjorklund, "Second-order cascading as the origin of large third-order effects in organic single-crystal-core fibers," *Opt. Lett.*, vol. 19, pp. 868–870, 1994.

[21] D. Marcuse, *"Theory of Dielectric Optical Waveguides,"* 2nd ed. San Diego, CA: Academic, 1991, ch. 1.

[22] W. Torruellas, G. Krijnen, D. Kim, R. Schiek, G. Stegeman, P. Vidakovic, and J. Zyss, "Cascading nonlinearities in an organic single crystal core fiber: The Čerenkov regime," *Optics Commun.*, vol. 112, pp. 122–130, 1994.

[23] T. C. Kowalczyk, K. D. Singer, and P. A. Cahill, "Anomalous-dispersion phase-matched second harmonic generation in polymer waveguides," in *Proc. Conf. Las. Elec. Opt.*, Baltimore, MD, 1995, paper CFA5, vol. 15, pp. 372–373.

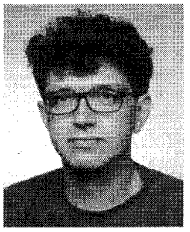

Gijs J. M. Krijnen (S'90–M'91) was born in 1961. He received the M.Sc. degree from the University of Twente following a study on magnetic recording carried out at the Philips Research Laboratories, Eindhoven, The Netherlands.

From 1987 to 1992, he carried out his Ph.D. research in the Lightwave Device Group of the MESA Research Institute at the University of Twente, Enschede, The Netherlands. In his Ph.D. work, he investigated modeling and implementation of nonlinear integrated optics devices. In 1992, he became a Fellow of the Royal Netherlands Academy of Arts and Sciences and studied the application of both second- and third-order nonlinearities in integrated optics sensors. In his current work, he coordinates a multidisplinary research program on low-cost components for small scale optical networks.

William Torruellas (S'84–M'90) received the M.S. degree in the Fall of 1987 and the Ph.D. degree in physics in June 1991, both from the Optical Sciences Center, University of Arizona. Currently, he is Senior Research Associate at the Center for Research and Education in Optics and Lasers, University of Central Florida. He is involved in research on optical properties of bulk, thin film, and single crystal fibers, mostly based on organic materials. His current interests include nonlinear wave propagation, nonlinear optics and spectroscopy, organics materials modeling, and near-infrared generation and detection. He has worked on 3–5 micron wavelength diode pumped OPO's, near- infrared nonlinear spectroscopic characterization of polymer thin films, characterization of the nonlinear optical properties of polysilane thin films and on near-infrared intracavity-laser-spectroscopy.

Dr. Torruellas is the recipient of several postdoctoral (NSF-NATO, NCR-NASA, NSF-FCE) fellowships and (Kodak, SPIE) scholarships. He has authored over 40 refereed publications. He is a member of OSA, SPIE, and AAAS.

George I. Stegeman (M'73) received the Ph.D. degree in physics in 1969 from the University of Toronto, Toronto Canada. From 1969 to 1980, he was a Professor at the University of Toronto working on nonlinear acoustic and optical wave interactions. He joined the Optical Sciences Center of the University of Arizona as a full Professor in 1980 where he worked primarily on nonlinear optics at waveguides and surfaces. In 1990, he came to CREOL of the University of Central Florida as the Cobb Family Chair in Optical Sciences and Enginerring, and holds tenured joint appointments in the Physics and Electrical Engineering Departments. His current interests include novel ultrafast nonlinear materials and their characterization over broad spectral regions, nonlinear optical devices in integrated and fiber optic waveguides, nonlinear polymers and signal processing in the optical domain.

Dr. Stegeman is the recipient of the Hertzberg Medal for Achievement in Physics of the CAP and is a Fellow of the Optical Society of America. He has 517 career publications and 2 books. He was Chair of the 1977 and 1982 Annual OSA meetings, QELS'93, the first and fourth Topical Meeting on Nonlinear Guided Wave Phenomena, and Co-Chair for ICONO'3 and ACS/OSA Topical Meeting on Organic Thin Films (1995–1996); numerous CLEO, IQEC, OSA, SPIE, IPR conference committees; Board of Directors of OSA and numerous society committees; Editorial Boards of Optics Letters, Editor for JOSA B, Optics Communications, and the Journals of Optical and Quantum Electronics, Optical Materials and Nonlinear Optics.

Hugo J. W. M. Hoekstra (M'94) was born in 1949. He received the M.Sc. degree in experimental physics from the University of Amsterdam in 1977.

After working as a teacher in high school, he began a Ph.D. study on magneto-optical properties of solid transition-metal halides at the University of Groningen where he received the Ph.D. degree in 1984. Between 1984 and 1988, he was a Postdoctoral Fellow in the field of surface science at the Universities of Nijmegen and Groningen. In 1988, he joined the Lightwave Device Group of the MESA Research Institute at the University of Twente, Enschede, The Netherlands, where he is engaged in work on linear and nonlinear integrated optics.

Paul V. Lambeck was born in 1939. He received the M.Sc. degree in physical chemistry from the University of Amsterdam in 1964.

In the same year, he joined the University of Twente, Enschede, The Netherlands, starting in the field of ferroelectric materials, a study which resulted in his Ph.D. dissertation. Since 1984, he has been an Associate Professor in the Lightwave Device Group of the MESA Research Institute at the University of Twente, Enschede, The Netherlands. His current interest is in the field of integrated optics and concentrates mainly on optical sensors and nonlinear devices.